Computers and Concrete, *Vol. 33, No. 6 (2024) 725-738*
https://doi.org/10.12989/cac.2024.33.6.725

Finite element modeling of reinforced and prestressed concrete panels under far-field blast loads using a smeared crack approach

Andac Lulec[1a], Vahid Sadeghian*[2] and Frank J. Vecchio[3b]

[1]*LARSA Inc., Melville, NY, USA*
[2]*Department of Civil and Environmental Engineering, Carleton University, Ottawa, ON, Canada*
[3]*Department of Civil and Mineral Engineering, University of Toronto, Toronto, ON, Canada*

(*Received November 11, 2022, Revised January 12, 2023, Accepted November 15, 2023*)

Abstract. This study presents a macro-modeling procedure for nonlinear finite element analysis of reinforced and prestressed concrete panels under blast loading. The analysis procedure treats cracked concrete as an orthotropic material based on a smeared rotating crack model within the context of total-load secant stiffness-based formulation. A direct time integration method compatible with the analysis formulation is adapted to solve the dynamic equation of motion. Considerations are made to account for strain rate effects. The analysis procedure is verified by modeling 14 blast tests from various sources reported in the literature including a blast simulation contest. The analysis results are compared against those obtained from experiments, simplified single-degree-of-freedom (SDOF) methods, and sophisticated hydrocodes. It is demonstrated that the smeared crack macro-modeling approach is a viable alternative analysis procedure that gives more information about the structural behavior than SDOF methods, but does not require detailed micro-modeling and extensive material characterization typically needed with hydrocodes.

Keywords: blast loading; computer modeling; concrete slabs; nonlinear analysis

1. Introduction

The need for accurate and practical analysis procedures for reinforced concrete (RC) structures subjected to blast is growing with the increasing number of military facilities, nuclear power plants, and industrial facilities being built around the world. The topic retains significance amongst researchers and designers due to a seemingly increasing number of natural and accidental hazards such as the recent industrial blast in Beirut that caused 204 deaths and about $15 billion in property damage. Existing blast analysis procedures available in the literature are mainly based on either simplified single-degree-of-freedom (SDOF) methods or highly sophisticated hydrocodes. SDOF procedures have been extensively used for design purposes to obtain maximum displacements and reactions under a given blast load. Studies undertaken to evaluate the accuracy of SDOF analysis methods by modeling experimental test specimens have produced mixed results; the accuracy of the analyses tend to be highly dependent on the structural and material modeling decisions made in simplifying the system to one DOF. For example, Dunkman *et al.* (2009) used two different SDOF analysis methods to calculate the maximum displacement of four prestressed concrete panels tested under simulated blast loads produced by a shock tube. One method assumed a bilinear load-deflection response, while the other method used a nonlinear model based on the secant slope of the moment-curvature diagram. The models overestimated the maximum deflection to some extent which was attributed to the simplification made in modeling end support conditions. In another study, Jacques (2011) developed a simplified blast analysis method and verified it against RC slab and wall specimens retrofitted with externally bonded fibre-reinforced polymer (FRP) composites. The analysis method solved the dynamic equation of motion for a SDOF system based on predefined force-deformation characteristics of the specimens. The analysis was able to adequately capture the overall response characteristics of the specimens. Recently, Yan *et al.* (2020) proposed a nonlinear SDOF model to calculate the maximum displacement of RC columns under close-in blast loading which was capable of accounting for the effect of axial load. The model, however, required conducting a fully coupled Euler-Lagrange interaction simulation prior to the SDOF analysis to estimate the blast pressure imposed on the column. In addition to SDOF models, there are other types of simplified analysis methods developed to assess the blast performance of concrete structures. Examples include development of a hysteretic moment-curvature relationship for analysis of RC flexural members under blast loading (Park *et al.* 2021) and development of an artificial neural network trained for prediction of spall characteristics of concrete columns and slabs subjected to blast loads (Dauj 2020).

Despite being computationally fast and easy to use,

*Corresponding author, Assistant Professor
E-mail: vahid.sadeghian@Carleton.ca
[a]Ph.D.
E-mail: andaclulec@gmail.com
[b]Professor Emeritus
E-mail: frank.vecchio@utoronto.ca

ISSN: 1598-8198 (Print), 1598-818X (Online)

simplified methods have some drawbacks which limit their application and accuracy. These methods often have difficulty representing important behavioral mechanisms such as dynamic effects, interactions between different force components (shear, axial, and bending), membrane action in slabs, crack patterns, and damage conditions. To overcome these limitations and evaluate structural performance in more detail, highly sophisticated hydrocodes implemented in finite element (FE) analysis software such as LS-DYNA and Abaqus are often used for research, specialized design, or safety assessment of existing structures.

Hydrocodes enable modeling fluid particles and shock waves and their interactions with a structure using various mesh descriptions. Some studies in the literature used the Coupled Eulerian-Lagrangian (CEL) method in which the explosive charge and ambient atmosphere were modeled with a Eulerian mesh, while the structure was modeled with a Lagrangian mesh allowing the consideration of solid-fluid interaction effects. For example, Lin *et al.* (2008) employed the CEL method to study the spalling mechanism in concrete slabs under contact detonation. Tai *et al.* (2011) used a similar modeling approach to study the propagation of blast pressure waves and the dynamic response of RC slabs under air blast loads. Zhao *et al.* (2013) assessed damage progression in square RC slabs under blast loads. Recently, Iannitti *et al.* (2018) analyzed the response of RC slabs under indoor explosions using the CEL method. Some other studies applied the blast pressure as a pre-determined pressure-time curve on the structure instead of modeling the fluid and wave propagation. Xu and Lu (2006) developed a 3D FE model using LS-DYNA to establish spallation criteria for different levels of damage in RC walls. They defined pressure-time curves using empirical blast models. Lin *et al.* (2014) used a similar modeling approach to investigate the effects of parameters such as dynamic material properties and reinforcement ratio on the blast response of RC panels. Nam *et al.* (2016) evaluated the blast performance of FRP-retrofitted RC walls using LS-DYNA. Gang and Kwak (2017) presented a tensile criterion based on the fracture energy theory to minimize the mesh-dependency in blast analysis of RC beams. Kong *et al.* (2018) developed a 3D FE model using LS-DYNA to assess the blast performance of RC slabs repaired with FRP composites. Jain and Chakraborty (2018) employed FE analysis to study the behaviour of basalt fiber reinforced concrete lining in tunnels subjected to internal blast loading. The blast load was simulated using the equivalent pressure-time curves obtained through hydrocode analyses. Rashad and Yang (2019) proposed a 3D nonlinear FE model to simulate the hyperdynamic behaviour and crack propagation in simply supported plain concrete slabs under blast loads. Gangolu *et al.* (2022) and Gangolu *et al.* (2023) used LS-DYNA to generate an analytical database for reinforced and prestressed concrete panels with various design parameters subjected missile impact. They then enhanced the analytical database with experimental test data to develop performance-based probabilistic models for prediction of missile-impact effects on concrete panels. Bhuyan and Sharman (2024) followed a similar approach to develop probabilistic capacity models for normal reinforced concrete and ultra-high strength concrete panels subjected to contact blast loading. Using the probabilistic capacity models, they were able to perform fragility analysis to evaluate the blast performance of concrete panels.

With hydrocodes, accurate simulation of the structural response typically requires highly detailed models with extremely fine finite element meshes with tens of thousands of elements which can make the modeling process tedious and result in excessively long analysis times. In addition, hydrocodes often require extensive characterization of material properties which are typically unknown. For example, a typical concrete material model in LS-DYNA requires between 12 to 50 input parameters, many of which are difficult to estimate and need additional material testing such as parameters related to fracture energy, tensile strength, yield surface, residual damage, and softening behavior. Brannon and Leelavanichkul (2009) compared four commonly used concrete damage plasticity models in LS-DYNA and demonstrated that the accuracy of the models can heavily depend on using well-tuned input parameters. Furthermore, the majority of the concrete material models in LS-DYNA are unable to represent crack propagation in concrete. To simulate physical cracks in concrete, an erosion model is typically used to delete concrete elements when the strain or stress reaches a critical value (Thiagarajan *et al.* 2015). Depending on the selected erosion criteria and limits, the structural response and crack pattern can be different.

This study presents an alternative analysis procedure, developed based on the Disturbed Stress Field Model (DSFM) (Vecchio 2000), for reinforced and prestressed concrete structures subjected to far-field blast loading. The analysis procedure was originally developed and incorporated into a nonlinear finite element analysis program, VecTor3, by Vecchio and Selby (1991) for 3D modeling of RC structures under static loads. Over the years, the analysis capabilities of VecTor3 have been extended to more advanced research areas such as fibre-reinforced concrete and steel-concrete composite materials as well as fire and fatigue loads (ElMohandes and Vecchio 2016, Isojeh *et al.* 2019). Recently, VecTor3 is enhanced with dynamic analysis capability under extreme loading conditions such as blast and impact. Development of such analysis capability required several changes to the analysis framework including implementation of a time integration method that is compatible with the secant stiffness-based formulation used in the original analysis procedure, implementation of an impulse loading function, and consideration of the effect of loading rate on material behaviour. This paper aims to assess the accuracy of the proposed analysis procedure to predict the blast behaviour of concrete slabs by conducting a comprehensive validation study on 14 blast tests. The paper first provides an overview of the analysis formulation and modeling approach followed by a description of the validation study. The study shows that by using simple finite element meshing techniques with reasonable mesh sizes and predefined material models which require only basic input parameters, the proposed analysis procedure can represent the behavior

of concrete slabs under blast with good accuracy. The proposed analysis procedure gives more information about the structural behavior than SDOF methods without requiring detailed micro-modeling and extensive material characterization typically needed with hydrocodes.

2. Overview of the analysis framework

2.1 Finite element formulation

The analysis framework is developed based on the Disturbed Stress Field Model (DSFM) (Vecchio 2000). The DSFM is a smeared rotating crack model in which cracked concrete is represented as an orthotropic material in the principal stress/strain directions using a secant stiffness-based formulation. Equilibrium, compatibility, and constitutive relationships are formulated in terms of average stresses and strains within a macro-modeling framework. In this analysis framework, the constitutive relation of the reinforced concrete material is expressed as

$$\{\sigma\} = [D]\{\varepsilon\} - \{\sigma^o\} \tag{1}$$

where $\{\sigma\}$ and $\{\varepsilon\}$ are the total stress and strain vectors, $[D]$ is the composite material stiffness matrix, and $\{\sigma^o\}$ is the pseudo-stress vector corresponding to the strain offsets defined as per the DSFM model (Vecchio 2000). The total strains of the concrete are composed of 1) net strains, $\{\varepsilon_c\}$, which are used for calculations of stresses and stiffness moduli; 2) elastic offset strains, $\{\varepsilon_{co}\}$, due to lateral expansion, thermal, and shrinkage; 3) plastic offset strains, $\{\varepsilon_{cp}\}$, due to permanent deformation resulting from high-level or cyclic loading; and 4) crack slip offset strains, $\{\varepsilon_{cs}\}$, due to shear slip on the crack. The total concrete strains can be represented as

$$\{\varepsilon\} = \{\varepsilon_c\} + \{\varepsilon_{co}\} + \{\varepsilon_{cp}\} + \{\varepsilon_{cs}\} = \{\varepsilon_{xx} \quad \varepsilon_{yy} \quad \varepsilon_{zz} \quad \gamma_{xy} \quad \gamma_{xz} \quad \gamma_{yz}\}^T \tag{2}$$

Assuming perfect bond between the reinforcement and the concrete, the total strains developed in the ith reinforcement component are equal to the total strains of the concrete at the same location. Therefore, in a similar manner, the total strains in the reinforcement can be expressed as a summation of: 1) net strains, $\{\varepsilon_s\}$; 2) elastic offset strains, $\{\varepsilon_{so}\}$, due to thermal and prestrain effects; and 3) plastic offset strains, $\{\varepsilon_{sp}\}$, due to steel yielding and damage resulting from cyclic loading. The total reinforcement strains can be written as

$$\{\varepsilon\}_i = \{\varepsilon_s\}_i + \{\varepsilon_{so}\}_i + \{\varepsilon_{sp}\}_i = \{\varepsilon_{xx} \quad \varepsilon_{yy} \quad \varepsilon_{zz} \quad \gamma_{xy} \quad \gamma_{xz} \quad \gamma_{yz}\}_i^T \tag{3}$$

From the strain state given in Eq. (2), the concrete principal net strains (ε_{c1}, ε_{c2}, ε_{c3}) can be computed using the strain transformation equations derived from Mohr's circle. Knowing the principal net strains in concrete, the principal stresses (f_{c1}, f_{c2}, f_{c3}) can be determined from a set of constitutive stress-strain relationships. In this study, the uniaxial compressive response of concrete is calculated based on the Hoshikuma *et al.* (1997) model. The compression softening effect in concrete is taken into account using the Vecchio and Collins (1993) model. The post-cracking tensile strength of concrete is calculated based on the tension stiffening model proposed by Bentz (2005). The cyclic response of concrete is considered using the model developed by Vecchio and Palermo (2003).

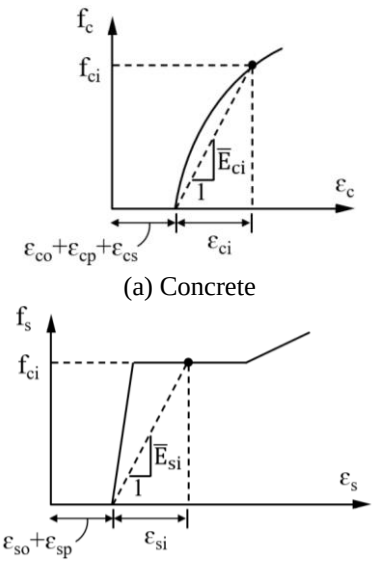

(a) Concrete

(b) Reinforcement

Fig. 1 Definition of secant moduli in the stress-strain response of concrete and reinforcement

Using the net strain in the ith component of the reinforcement (ε_{si}) computed from Eq. (3) and a constitutive stress-strain relationship, the corresponding stress in the reinforcement (f_{si}) can be determined. In this study, the cyclic response of reinforcement is calculated using the Seckin (1981) model which consists of a trilinear backbone stress-strain relationship, a linear unloading response, and a nonlinear reloading response with the Bauschinger effect. Also, the inelastic buckling of reinforcement is taken into account using the Akkaya *et al.* (2019) model. For more details about the material behavioral models, refer to Lulec (2017).

By using the principal strains and stresses, the concrete secant moduli in the principal directions ($\bar{E}_{c1}$, $\bar{E}_{c2}$, $\bar{E}_{c3}$) and the secant shear moduli ($\bar{G}_{c12}$, $\bar{G}_{c13}$, $\bar{G}_{c23}$) are calculated as

$$\bar{E}_{c1} = \frac{f_{c1}}{\varepsilon_{c1}};\ \bar{E}_{c2} = \frac{f_{c2}}{\varepsilon_{c2}};\ \bar{E}_{c3} = \frac{f_{c3}}{\varepsilon_{c3}} \tag{4}$$

$$\bar{G}_{c12} = \frac{\bar{E}_{c1}\bar{E}_{c2}}{\bar{E}_{c1}+\bar{E}_{c2}};\ \bar{G}_{c13} = \frac{\bar{E}_{c1}\bar{E}_{c3}}{\bar{E}_{c1}+\bar{E}_{c3}};\ \bar{G}_{c23} = \frac{\bar{E}_{c2}\bar{E}_{c3}}{\bar{E}_{c2}+\bar{E}_{c3}} \tag{5}$$

Fig. 1 demonstrates the definition of secant moduli in the stress-strain response of concrete and reinforcement.

The concrete material stiffness matrix in the principal stress directions is expressed in terms of the secant moduli as follows

$$[D_c'] = \begin{bmatrix} \bar{E}_{c1} & 0 & 0 & 0 & 0 & 0 \\ 0 & \bar{E}_{c2} & 0 & 0 & 0 & 0 \\ 0 & 0 & \bar{E}_{c3} & 0 & 0 & 0 \\ 0 & 0 & 0 & \bar{G}_{c12} & 0 & 0 \\ 0 & 0 & 0 & 0 & \bar{G}_{c13} & 0 \\ 0 & 0 & 0 & 0 & 0 & \bar{G}_{c23} \end{bmatrix} \tag{6}$$

In this formulation, Poisson's effects and material dilations are represented as elastic or plastic offset strains; hence Eq. (6) can be written in the form of a diagonal matrix. The concrete material matrix can be transformed from the principal directions to the material local coordinates using the following equation

$$[D_c] = [T_c]^T [D_c'][T_c] \tag{7}$$

where $[T_c]$ is the transformation matrix, calculated by using the directional cosines between the principal stress directions and material local coordinate system (Cook *et al.* 1989).

Employing a similar approach for the smeared reinforcement, the secant modulus and the reinforcement material matrix for the i[th] component of reinforcement are calculated as

$$\bar{E}_{si} = \frac{f_{si}}{\varepsilon_{si}};\ [D_s']_i = \begin{bmatrix} \rho_i \bar{E}_{si} & 0 & 0 & 0 & 0 & 0 \\ 0 & 0 & 0 & 0 & 0 & 0 \\ 0 & 0 & 0 & 0 & 0 & 0 \\ 0 & 0 & 0 & 0 & 0 & 0 \\ 0 & 0 & 0 & 0 & 0 & 0 \\ 0 & 0 & 0 & 0 & 0 & 0 \end{bmatrix} \tag{8}$$

where $\bar{E}_{si}$ and ρ_i are the secant modulus and the ratio of the i[th] reinforcement component, respectively. The reinforcement material matrix is transformed with a similar approach used in the transformation of the concrete material matrix, as expressed in Eq. (9). The transformation matrix $[T_s]_i$ is formed by using the directional cosines between the material local coordinates and the inclination of the reinforcement component.

$$[D_s]_i = [T_s]_i{}^T [D_s']_i [T_s]_i \tag{9}$$

Finally, the concrete material matrix and reinforcement material matrices are combined to form the total material stiffness matrix, $[D]$

$$[D] = [D_c] + \sum_{i=1}^{n} [D_s]_i \tag{10}$$

After the total material stiffness matrix is obtained, the element stiffness matrix, $[k]$, can be computed as

$$[k] = \int_{Vol} [B]^T [D][B] dV \tag{11}$$

where $[B]$ is the strain function matrix (Cook *et al.* 1989) specific for the element type being considered. In this study, eight-noded hexahedral elements are used to model concrete slabs. Lastly, the element stiffness matrices are assembled to form the global stiffness matrix for the whole structure.

2.2 Local analysis at the crack

A key feature of the analysis procedure presented here is its ability to account for local behavior at crack locations and compute shear stresses and deformations (i.e., shear slips) occurring on the surface of cracks. It is well-recognized that, because of bond effects between the concrete and reinforcement, average tensile stresses exist in the concrete between cracks (i.e., tension stiffening effect). To transfer the concrete tensile stresses across the crack

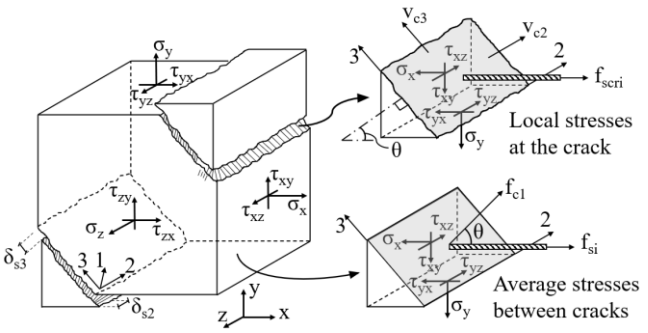

Fig. 2 Average and local stress conditions in RC elements after cracking

surface, it is required to have local increases in the reinforcement stresses. To ensure that the reinforcement is capable of carrying the concrete tensile stresses across the cracks, the DSFM model (Vecchio 2000) limits the tensile stress in concrete (f_{c1}) to

$$f_{c1} \le \sum_{i=1}^{n} \rho_i \left(f_{yi} - f_{si}\right) \cos^2 \theta_{1i} \tag{12}$$

where f_{yi} is the yield stress of the i[th] reinforcement component and θ_{1i} is the angle between the reinforcement direction and the principal one direction.

To maintain equilibrium in the directions perpendicular and parallel to the crack, shear stresses along the crack surface are developed to balance the localized increase in reinforcement stresses (f_{scri}), as shown in Fig. 2. Assuming that the rotating crack surface is perpendicular to the first principal tensile stress direction, shear stresses along the crack surface can be considered by their components in the second and third principal stress directions (v_{c2} and v_{c3}). The two shear stress components can be computed from the following equations

$$v_{c2} = \sum_{i=1}^{n} \rho_i (f_{scri} - f_{si})(l_i l_1 l_2 + m_i m_1 m_2 + n_i n_1 n_2) \tag{13}$$

$$v_{c3} = \sum_{i=1}^{n} \rho_i (f_{scri} - f_{si})(l_i l_1 l_3 + m_i m_1 m_3 + n_i n_1 n_3) \tag{14}$$

where f_{scri} is the local stress in the i[th] reinforcement component across the crack surface; (l_i, m_i, n_i) are direction cosines of a unit vector in the direction of the i[th] reinforcement component; and (l_1, m_1, n_1), (l_2, m_2, n_2), and (l_3, m_3, n_3) are direction cosines of a unit vector in the principal direction 1, 2, and 3, respectively.

The shear slip deformations (δ_{s2} and δ_{s3}) due to the shear stresses across the crack (v_{c2} and v_{c3}) are determined using the Walraven (1981) model. By dividing the slip deformations by the average crack spacing (s), slip shear strains in the second and third principal stress directions (γ_{s2} and γ_{s3}) are computed, as expressed in Eq. (15). The slip shear strains are then incorporated into the material calculation as elastic strain offsets defined in Eq. (2) and act on the concrete element as pseudo-stress values defined in Eq. (1).

$$\gamma_{s2} = \frac{\delta_{s2}}{s} \ and \ \gamma_{s3} = \frac{\delta_{s3}}{s} \tag{15}$$

2.3 Dynamic analysis method

A modified version of the Newmark's direct time integration method (Newmark 1959) compatible with the analysis formulation is adapted herein to solve the dynamic equation of motion. The equation of motion can be expressed in an incremental form as follows

$$m\Delta\ddot{u} + c(t)\Delta\dot{u} + k(t)\Delta u = \Delta p(t) \tag{16}$$

where $\Delta\ddot{u}$, $\Delta\dot{u}$, and Δu are changes in acceleration, velocity, and displacement during the time interval Δt, respectively. Similarly, $\Delta p(t)$ denotes the change in applied force. Also, *c* and *k* are damping and stiffness values at time *t*, respectively. Referencing a parameter at the beginning of a time interval with subscript *n*, and the parameter at the end of the interval with subscript *n*+1, incremental relations can be presented as

$$\begin{gathered}\Delta\ddot{u}_n = \ddot{u}_{n+1} - \ddot{u}_n;\ \Delta\dot{u} = \dot{u}_{n+1} - \dot{u}_n; \\ \Delta u = u_{n+1} - u_n;\ \Delta p = p_{n+1} - p_n\end{gathered} \tag{17}$$

According to the Newmark's method, velocity, $\dot{u}_{n+1}$, and displacement, u_{n+1}, at the end of the time interval are as follows

$$\dot{u}_{n+1} = \dot{u}_n + (1-\gamma)\Delta t\ddot{u}_n + \gamma\Delta t\ddot{u}_{n+1} \tag{18}$$

$$u_{n+1} = u_n + \Delta t\dot{u}_n + (0.5-\beta)\Delta t^2\ddot{u}_n + \beta\Delta t^2\ddot{u}_{n+1} \tag{19}$$

where γ and β are coefficients defining the variation of acceleration over the time step. In this study, the constant acceleration method (γ=0.50 and β=0.25) is used since it is unconditionally stable and therefore allows using longer time steps improving the computational performance of the proposed macro-modeling procedure. Substituting Eq. (17) into Eqs. (18) and (19), and solving for $\Delta\ddot{u}$ results in

$$\Delta\ddot{u} = \frac{1}{\beta\Delta t^2}\Delta u - \frac{1}{\beta\Delta t}\dot{u}_n - \frac{1}{2\beta}\ddot{u}_n \tag{20}$$

As discussed in the previous section, the analysis framework is developed using a total-load secant stiffness-based formulation. Newmark's time integration method, however, is based on the tangent stiffness. To make Newmark's method adaptable to the analysis framework, the original numerical solution of the dynamic equation of motion is modified to obtain a total-load secant stiffness-based formulation according to the work done by Saatci and Vecchio (2009). The incremental equation of motion given in Eq. (16) can be reorganized in terms of total loads and the secant stiffness as

$$m\ddot{u}_{n+1} + c_{n+1}\dot{u}_{n+1} + \bar{k}_{n+1}u_{n+1} = p_0 + p_{n+1} \tag{21}$$

where $\bar{k}$ is the secant stiffness and p_0 is the constant static load. By substituting Newmark's equations given in Eqs. (18) and (19) into Eq. (21), the previous equation becomes

$$\begin{gathered}m(\ddot{u}_n + \Delta\ddot{u}) + c_{n+1}(\dot{u}_n + \Delta t\ddot{u}_n + \gamma\Delta t\Delta\ddot{u}) + \\ \bar{k}_{n+1}u_{n+1} = p_0 + p_{n+1}\end{gathered} \tag{22}$$

After Eq. (20) is substituted into Eq. (22) and reorganized into matrix form, the following equation for dynamic analysis can be obtained

$$\left(\left[\bar{k}_{n+1}\right] + \left[k^*_{n+1}\right]\right)\{u_{n+1}\} = \{p_0\} + \{p^*_{n+1}\} \tag{23}$$

where

$$\left[k^*_{n+1}\right] = \frac{[m]+[c_{n+1}]\gamma\Delta t}{\beta\Delta t^2} \tag{24}$$

$$\begin{gathered}\{p^*_{n+1}\} = \{p_{n+1}\} + \frac{[m]+[c_{n+1}]\gamma\Delta t}{\beta}\left(\frac{\{u_n\}}{\Delta t^2} + \frac{\{\dot{u}_n\}}{\Delta t} + \frac{\{\ddot{u}_n\}}{2}\right) - \\ [c_{n+1}](\{\dot{u}_n\} + \Delta t\{\ddot{u}_n\}) - [m]\{\ddot{u}_n\}\end{gathered} \tag{25}$$

It is worth noting that Eq. (23) follows the same format as the Hookes' law equation used for static analyses (i.e., force equals to stiffness times displacement). As a result, the Newmark's method can be used in the total-load secant stiffness-based formulation framework to carry out dynamic analyses through the use of a static analysis procedure.

In the proposed dynamic analysis procedure, the total mass of a structure is evenly distributed to the nodes of the FE model and is represented by a diagonal mass matrix. The lumped masses are assigned to the eight-noded hexahedral and six-noded wedge elements which are the two concrete element types available in the VecTor3 analysis software. In dynamic analyses, damping is usually used to include additional energy dissipating mechanisms and to reduce the instability of numerical solutions. Because of the short duration of blast, however, the damping has less effect and is only important for capturing the post-blast response characteristics of structures (e.g., residual displacement and damage). In this study, almost all of the energy dissipation is introduced through the nonlinear concrete and reinforcing steel hysteresis models due to inherent characteristics of materials; only a small amount of damping is required to stabilize the dynamic analysis which is defined according to Rayleigh damping

$$[C] = a_0[m] + a_1[k] \tag{26}$$

In this equation, the damping matrix, $[C]$, is proportional to the mass, $[m]$, and stiffness, $[k]$, matrices. a_0 and a_1 are coefficients for the mass and stiffness matrices, respectively, determined from modal damping ratio and angular frequency of two arbitrary modes of the structure.

The analysis follows an iterative procedure. First, the static secant stiffness matrix is computed based on a set of assumed nodal displacements using the relationships provided in the Overview of the Analysis Framework section. By calculating the damping and mass matrices, the dynamic stiffness matrix and force vector can also be determined from equations presented in this section. Knowing the total force vector and stiffness matrix resulted from both static and dynamic effects, new nodal displacements can be obtained by solving Eq. (23). If the new displacements are within a predefined error limit from the assumed displacements, the analysis is considered to have converged and it proceeds to the next time step. Otherwise, the analysis procedure is repeated until displacements converge, or a predefined maximum number of iterations are performed. The analysis first will be conducted using small damping ratios to avoid introducing excessive damping to the system. If there is a numerical instability in the analysis, the damping ratios will be gradually increased to facilitate convergence of displacements. Fig. 3 demonstrates an overview of the analysis procedure. The analysis steps implemented into VecTor3 for dynamic simulation are shown in red.

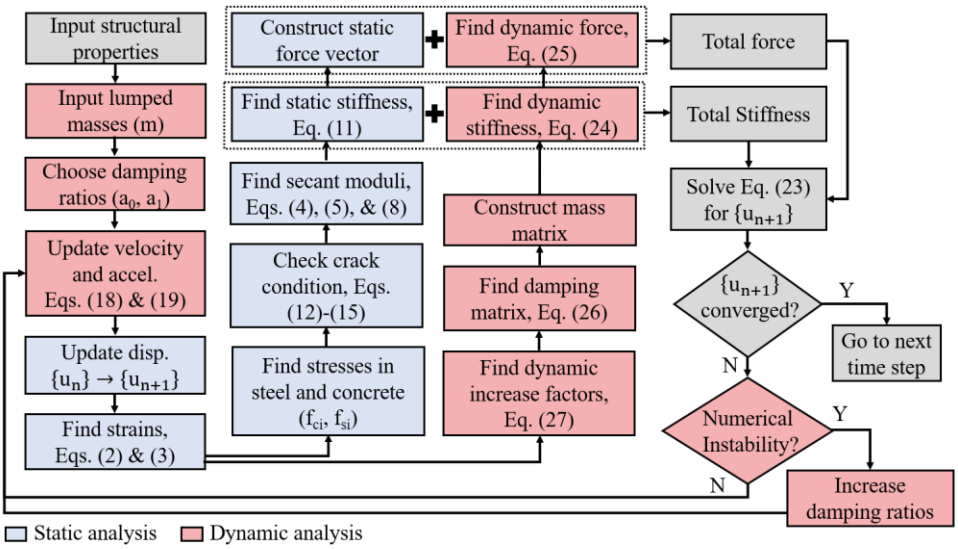

Fig. 3 Overview of the analysis procedure (steps added for dynamic analysis are shown in red)

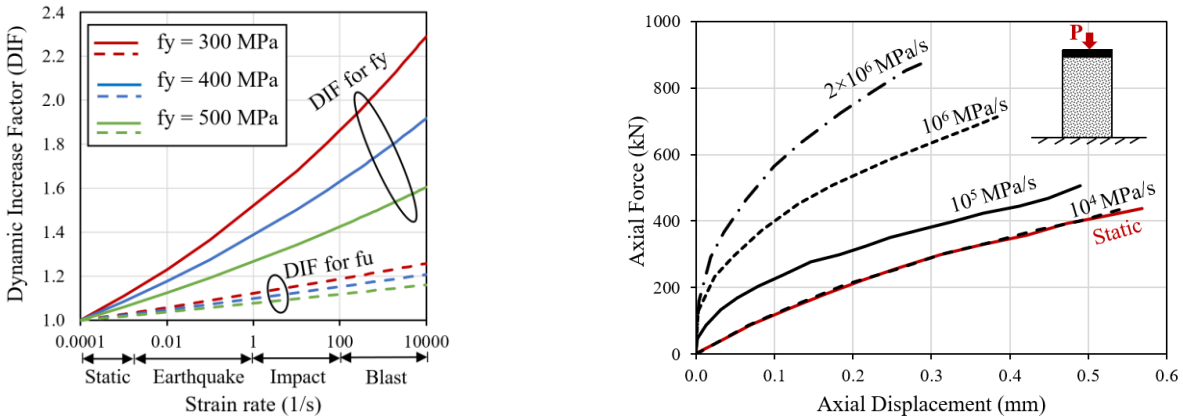

Fig. 4 Consideration of Strain rate effect in the analysis procedure for (a) Steel based on Malvar and Crawford (1998) model and (b) Concrete based on the confining stresses due to inertia

2.4 Strain rate effects

The behavior of steel and concrete which are rate-dependent materials is different under blast loads compared to that under static loads because of the high loading rate of blast events. This effect, which is commonly known as the strain rate effect, results in an increase in the strength and stiffness of materials as the loading rate increases. In this study, the Malvar and Crawford (1998) formulations were implemented into the analysis framework to model strain rate effects for steel. This model increases the yield and ultimate strength of steel according to the dynamic increase factor (DIF) calculated from Eq. (27).

$$DIF = \left(\frac{\dot{\varepsilon}_s}{10^{-4}}\right)^{\alpha_y \text{ or } \alpha_u} \quad (27)$$

where $\dot{\varepsilon}_s$ is the strain rate that can be estimated from strain values in the current and previous time steps, and α_y and α_u are the yield and ultimate strength factors determined from Eq. (28). Fig. 4(a) demonstrates how the DIF for the yield and ultimate strength of steel changes as the strain rate increases.

$$\alpha_y = 0.074 - 0.040\frac{f_y}{414} \text{ and } \alpha_u = 0.019 - 0.009\frac{f_y}{414} \quad (28)$$

Consideration of strain rate effects for modeling concrete material has been the subject of several discussions in the research literature. Although the results obtained from experimental tests demonstrate an increase in the concrete strength as the loading rate increases, some researchers argue that whether this strength gain should be included as a separate phenomenon in the analysis procedure. Li and Meng (2003) found that majority of the strength gain observed in high strain rate tests resulted from confining stresses developed in test specimens due to lateral inertia. Therefore, if an analysis method accounts for both the strength gain due to the strain rate effect and confining stresses due the inertia, it can overestimate the concrete strength. To further investigate this point, Cotsovos and Pavlovic (2008) modeled and analyzed concrete elements under high strain rates and observed a strength increase with only considering the confining stresses due to the lateral inertia. The analysis procedure proposed in this study is capable of calculating the triaxial confining stresses

induced by the inertia of the structure and therefore no additional strength increase factor needs to be considered for concrete in the formulation. The concrete confinement effect is taken into account by increasing both the uniaxial compressive strength (f'_c) and the corresponding strain (ε_0) by a strength enhancement factor (β_l) determined from Eq. (29) which was initially proposed by Kupfer *et al.* (1969) and later improved by Richart *et al.* (1928).

$$\beta_l = \left[1 + 0.92\left(\frac{f_{cn}}{f'_c}\right) - 0.76\left(\frac{f_{cn}}{f'_c}\right)^2\right] + 4.1\left(\frac{f_{cl}}{f'_c}\right) \quad (29)$$

where f_{cl} is the lateral confining stress and f_{cn} is the difference in normal lateral stresses acting on the concrete, both determined from stresses in the principal directions.

To demonstrate the effect of confining stresses due to inertia in the proposed analysis procedure, a 300 mm×150 mm concrete cylinder with the uniaxial compressive strength of 25 MPa was modeled using hexahedral elements. The mass was distributed to all nodes of the model. The external load was applied as a nodal force monotonically increased at each time step until the cylinder failed under compression. By reducing the analysis time step, the loading rate varied from 10^4 MPa/second to 2×10^6 MPa/second. The axial force-displacement response of the cylinder computed at different loading rates is shown in Fig. 4(b). It can be seen that as the loading rate increases the strength of cylinder increases even though no DIF is considered in the model. The increase in strength is a result of inertia forces that are imposed on the structure at high loading rates which lead to confining stresses that restrict the deformations in the axial and lateral directions. The results show that the proposed analysis procedure is capable of capturing the loading rate effect on concrete without requiring any additional consideration.

3. Validation study

A comprehensive validation study is conducted to evaluate the accuracy of the presented dynamic analysis procedure for computing the response of reinforced and prestressed concrete slabs subjected to far-field blast loading. The specimens were selected from four series of blast tests carried out at the University of Texas, University of Ottawa, and U.S. Army Engineer Research and Development Center. A brief description of the test specimens, FE modeling procedure, and analysis results is provided in the following.

It should be noted that all analyses were conducted using the same material models and analysis parameters and no attempt was made to fine tune the results. The material models were defined using only basic input parameters: uniaxial compressive strength, strain at peak compressive strength, and Young's modulus for the concrete; and bar diameter, yield strength, ultimate strength, Young's modulus, strain hardening strain, ultimate strain, and initial prestressing strain for the reinforcing steel. The case studies presented in this study all have flexural dominant behavior and therefore no element erosion criteria were needed for their analyses. Element erosion is typically used to model the localized damage condition of the target. In the proposed analysis procedure, however, crack width and angle calculations inherently included in the constitutive models used by DSFM are sufficient for capturing the localized damage in panels with flexural dominant behavior.

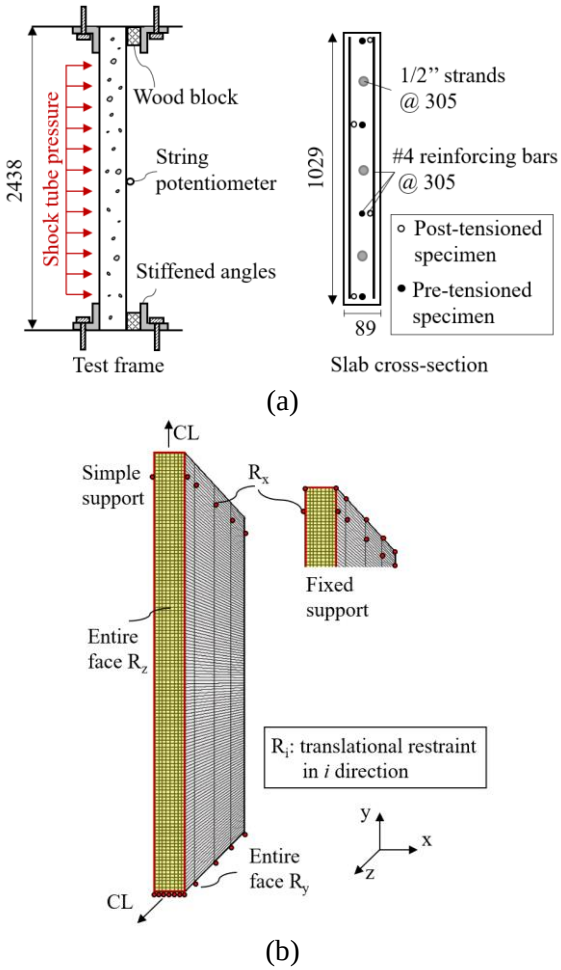

Fig. 5 (a) Details of pre- and post-tensioned slabs tested by Dunkman *et al.* (2009) and (b) The corresponding FE model (right) (all dimensions in mm; 1 mm=0.0394 in.)

Table 1 Blast load characteristics for tests conducted by Dunkman *et al.* (2009)

Blast Load	Pressure (kPa)	Duration (ms)	Impulse (kPa.ms)
B1	43	13.3	290
B2	72	15.4	552
B3	76	34.5	1310

3.1 University of Texas specimens

Dunkman *et al.* (2009) conducted a test series where a pre-tensioned and a post-tensioned slab were subjected to three blast loads with increasing intensity (Blast 1, 2, and 3). The test specimens were 2578×1029×89 mm (101.49×40.51×3.50 in.) in size with a clear span of 2438 mm (95.98 in.). The concrete had a compressive strength of

Table 2 Comparison of experimental and analytical results for positive phase of blast loads

Blast Load	Specimen	Max. Positive Deflection (mm)							
		Test	SDOF Methods		Proposed FE Procedure		SDOF Methods/Test	Proposed FE Procedure-Pinned /Test	Proposed FE Procedure-Fixed/Test
			M1	M2	Pinned End	Fixed End			
B1	Pre-T	5.6	13.5	12.4	11.3	6.8	2.3	2.0	1.2
	Post-T	4.3	13.5	12.4	10.8	4.1	3.0	2.5	1.0
B2	Pre-T	24.4	29.0	29.0	33.2	25.1	1.2	1.4	1.0
	Post-T	27.2	29.0	29.0	32.2	23.1	1.1	1.2	0.8
B3	Pre-T	66.0	101	98.8	70.0	54.2	1.5	1.1	0.8
	Post-T	94.5	101	98.8	79.5	68.5	1.1	0.8	0.7

*The end support condition that resulted in more accurate results is highlighted in gray

Table 3 Comparison of experimental and analytical results for negative phase of blast loads

Blast Load	Specimen	Max. Positive Deflection (mm)					
		Test	SDOF Methods	Proposed FE Procedure		SDOF Methods/Test	Proposed FE Procedure-Pinned /Test	Proposed FE Procedure-Fixed/Test
				Pinned End	Fixed End			
B1	Pre-T	20.1	NA	16.6	12.3	NA	0.8	0.6
	Post-T	21.3		16.5	12.5		0.8	0.6
B2	Pre-T	26.9		28.4	23.6		1.1	0.9
	Post-T	28.4		30.7	16.8		1.1	0.6
B3	Pre-T	14.7		12.8	11.5		0.9	0.8
	Post-T	14.5		16.4	8.1		1.1	0.6

*The end support condition that resulted in more accurate results is highlighted in gray

30.8 MPa (4.47 ksi). Grade 60 steel rebars were used for the in-plane and transverse reinforcement. Additionally, Grade 270 strands were used as prestressing steel, and prestressed to 138 kN (31.02 kips). Details of the specimens are shown in Fig. 5. Table 1 also summarizes the characteristics of the blast loads applied to the specimens.

In addition to midspan displacement time-histories and crack conditions of the test specimens, results obtained from two simplified SDOF analyses were reported. These two methods were based on elastic-plastic models and enabled estimating the deflection of a specimen under a given blast load. While the first method used the average elastic stiffness of uncracked and cracked cross sections, the second method was based on the secant stiffness calculated from the moment-curvature response.

For the FE analysis, taking advantage of double symmetry, only one quarter of each slab was modeled to reduce the computational time. Appropriate boundary conditions were applied on the axes of symmetry to simulate the response of the entire specimen. The concrete was modeled using eight-noded hexahedral elements, while the in-plane, transverse, and prestressing steel were modeled with two-noded truss elements. Since the specimens were predominantly bent about one axis only, to increase the computational efficiency, a courser mesh was used in the plane perpendicular to bending plane, yielding a 10×10×150 mm (0.39×0.39×5.90 in.) mesh. For the pre-tensioned specimen, the prestressing steel was assumed to be perfectly bonded to the concrete elements. For the post-tensioned specimen, the prestressing steel was in lubricated sheathes, and thus it was modeled with two-noded non-dimensional link elements having no stiffness in the direction of the prestressing steel.

In the test, the slabs were supported by steel angles and wooden blocks providing an end restraint condition which was somewhere between the simply supported case and the fixed support case. Because the exact degree of fixity of the supports was unknown, both of the two boundary cases (the simple support case and the fixed support case) were analyzed. The actual response of the slabs was expected to be between these two cases. The FE model and the two end support cases are shown in Fig. 5. Blast loadings were modeled as a uniform pressure, and the impulse loads were calculated according to the tributary areas of the elements on the blast face. The analyses were performed using a time-step of 0.1 ms. To avoid introducing excessive damping to the FE model, the damping ratio was initially specified as 0.5% for the first two modes, and then it was gradually reduced until the analyses became numerically unstable. The lowest damping ratio at which the analyses were numerically stable was 0.1% for the first two modes.

Tables 2 and 3 compare the peak displacements of the specimen calculated by the proposed analysis procedure against those obtained from the experiments and the SDOF methods used by Dunkman *et al.* (2009). In general, the proposed procedure computed the peak displacements in the positive phase of the blast load with better accuracy compared to the SDOF methods. The results obtained from

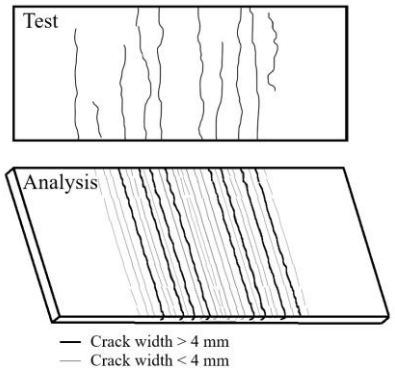

(a) Pre-tensioned specimen

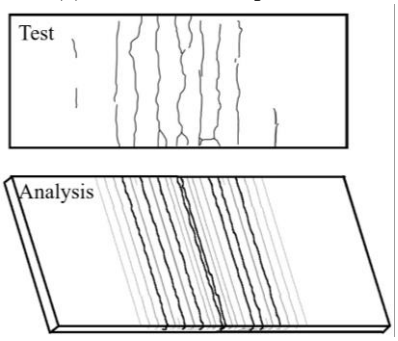

(b) Post-tensioned specimen

Fig. 6 Comparison of crack patterns obtained from tests and FE analysis for Dunkman *et al.* (2009) slabs

the SDOF methods were identical for both the pre-tensioned and post-tensioned specimens since the effect of prestressing technique was not accounted for in these methods. Another limitation of the SDOF methods is that they can not provide any information about the structural response under the negative (rebound) phase of blast load. The proposed analysis procedure, however, is able to consider the effect of prestressing technique and calculate the peak displacement in the rebound direction. For Blast 1 and 2 which had relatively low blast intensities, the FE model with the fixed support condition predicted the peak displacement in the blast direction with better accuracy compared to the model with the pinned support condition. Increasing the intensity of the blast load to Blast 3 reduced the degree of rotational fixity at the support provided by steel angles and wooden blocks and as a result the predictions of the model with the pinned support condition were better. In the rebound direction, the model with the pinned support condition estimated the peak displacements with better accuracy for all three blast intensities compared to the model with the fixed support condition. This is expected as when the specimen is subjected to the negative phase of blast load it has been already damaged due to the positive pressure phase which can reduce the degree of fixity at the end supports.

Another advantage of the proposed macro-modeling analysis procedure is that it can predict crack patterns and damage modes under blast loads. For the case study considered here, both FE models (the simple support and fixed support cases) produced similar crack patterns with the experiments in terms of location and type of the cracks.

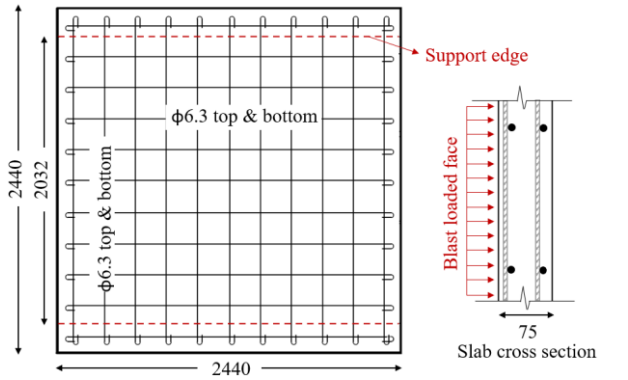

Fig. 7 Details of RC slab tested by Jacques (2011) (all dimensions in mm; 1 mm=0.0394 in.)

Fig. 6 compares the crack patterns obtained from the FE analysis and tests for both the pre-tensioned and post-tensioned specimens. It can be seen that the cracks were concentrated at the midspan of the panel, continued along the surface of the panel, and were perpendicular to the bending plane. The FE models computed larger cracks for the post-tensioned specimen than those for the pre-tensioned specimen, which is consistent with the experimental observations. For both specimens, the computed and experimentally observed behaviors were governed by flexure.

3.2 University of Ottawa specimen

Jacques (2011) tested a 2440×2440×75 mm (96.06×96.06×2.95 in.) slab specimen with a clear span of 2232 mm (87.87 in.) under three blasts with increasing intensity. The slab was clamped at the two edges by two steel angles representing a simple support case. Eleven 6.3 mm (0.25 in.) diameter reinforcing wires were used in both directions on each face as the longitudinal and transverse reinforcement. The dimensions and the details of the reinforcement are presented in Fig. 7. In addition to the experimental program, Jacques (2011) performed an analytical study to predict the peak displacement and its occurrence time using a simplified SDOF model.

The FE modeling procedure was similar to that described for the University of Texas specimens. The support conditions were modeled as simply supported. The concrete was modeled with 7320 hexahedral elements using a mesh size of 7×10×220 mm (0.27×0.39×8.66 in.). In addition to the hexahedral elements, 1524 truss elements were used to model the longitudinal and transverse reinforcement. A damping ratio of 0.5% was assigned for the first and second modes, which was the lowest value producing a stable solution for the post-blast response.

The information about the blast loads applied to the specimen and the peak displacements obtained from the tests, the proposed FE analyses, and the SDOF method are provided in Table 4. It can be seen that for all three blast intensities, the SDOF method overestimated the peak displacements, while the values computed by the FE analyses matched reasonably well with the experimental results. In terms of the crack pattern, the FE analysis for

Table 4 Comparison of experimental and analytical results for RC slab tested by Jacques (2011)

ID	Blast Load			Max. Displacement (mm)			SDOF Method/Test	Proposed FE Procedure/Test
	Reflected Pressure (kPa)	Duration (ms)	Reflected Impulse (kPa-ms)	Test	SDOF Method	Proposed FE Procedure		
B1	15.4	13.8	123.3	6.9	8.9	6.8	1.29	0.99
B2	28.2	14.7	204.2	16.3	18.6	17.1	1.14	1.05
B3	100.6	19.5	811.2	197.5	217.8	180.1	1.10	0.91
Average							1.18	0.98

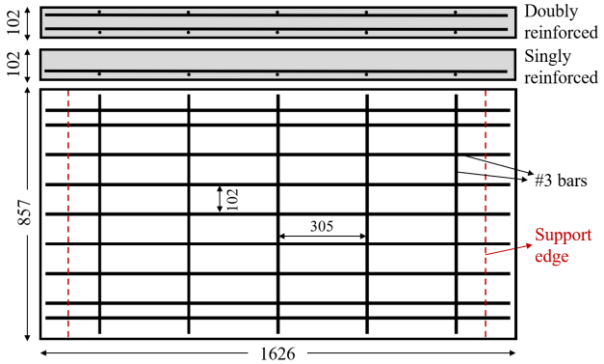

Fig. 8 Details of US Army singly and doubly reinforced slab specimens (dimensions in mm; 1 mm=0.0394 in.)

Blast 1 yielded flexural cracks concentrated at the midspan with a maximum width of 0.7 mm (0.027 in.) at the time of peak displacement and less than 0.1 mm (0.004 in.) at the residual state. As the intensity of the blast increased, the FE analysis computed distributed cracks along the slab. For Blasts 2 and 3, the maximum crack widths were 1.0 and 5.5 mm (0.039 and 0.216 in.), and the residual crack widths were 0.3 and 3.7 mm (0.012 and 0.146 in.), respectively. The computed crack widths and the overall behavior of the specimen under different blast loads were consistent with the experimental tests.

3.3 US Army doubly reinforced specimens

Robert and Johnson (2009) tested ten 1626×857×102 mm (64.01×33.74×4.01 in.) specimens under blast loads. The concrete strength of the specimens was either 26.7 or 107 MPa (3.87 or 15.52 ksi). The panels were doubly reinforced with #3 reinforcing bars with either Grade 60 reinforcement or High-Strength-Low-Alloy Vanadium (HSLA-V) reinforcement. The slabs were supported only in the longitudinal direction with steel tubes located on both sides of the specimen. The details of the specimen are presented in Fig. 8, where the center of the steel tubes is marked as the support edges.

In this study, Slabs 3, 5, and 9 were modeled since pressure-time histories for these slabs were reported in the experiment. In addition to the comparison of the analytical and experimental results, the proposed analysis procedure was compared against the numerical studies carried out by Thiagarajan *et al.* (2015) using the LS-DYNA analysis software. Among various mesh sizes and concrete constitutive models examined by Thiagarajan *et al.* (2015), the FE model with the Winfrith concrete model and a 12.7 mm (0.50 in.) mesh size provided the highest accuracy and therefore was selected for the comparison in this study. The FE model consisted of 69632 eight-noded hexahedral elements representing the concrete, and 3120 Hughes-Liu beam elements representing the reinforcement. The Concrete and reinforcement elements were connected through the Constrained Lagrange in Solid formulation assuming perfect bond between the two materials. The constant stress element formulation along with the Flanagan-Belytschko based hourglass control option (with the hourglass coefficient of 0.03) were used in the model. To represent the boundary condition of the test, the top and bottom nodes of the slab were restrained against movement in the vertical and out-of-plane directions. The input parameters used for the Winfrith concrete model were the mass density of 2400 kg/m^3, tangent modulus of 24.8 GPa, Poisson's ratio of 0.18, uniaxial compressive strength of 27.6 MPa, uniaxial tensile strength of 3.3 MPa, and fracture energy/crack width of 0.0002 J/mm^2. The rest of the input parameters was defined using automated parameter generation of LS-DYNA. The input parameters for the high strength concrete were the same as the normal strength concrete with the exception of the compressive and tensile strength values. The strain rate effect in concrete was considered using the CEB-FIB model (CEB-FIP 1993) which enhances the elastic, shear, and bulk moduli as well as the tensile and compressive strength of concrete. The reinforcement was modeled with a plastic kinematic model capable of considering the strain hardening effects. The material property values used for the reinforcement model were the mass density of 7830 kg/m^3, Young's modulus of 200 GPa, Poisson's ratio of 0.3, yield strength of 572 MPa, and tangent modulus of 20 GPa.

With the proposed analysis procedure, only a quarter section of the specimen was modeled due to double symmetry, as done with previous specimens modeled in this study. The support conditions were modeled as simply supported. 6048 hexahedral elements, with a mesh of 7×20×50 mm (0.27×0.79×1.97 in.), were used to represent the concrete components of the slabs. Additionally, the longitudinal and transverse reinforcement was modeled with 458 truss elements. Only the basic input parameters mentioned at the beginning of the Validation Study were used to define the material models.

The midspan displacement-time histories obtained from the experiment and the FE analyses are shown in Fig. 9. As can be observed from the figure, the analytical responses

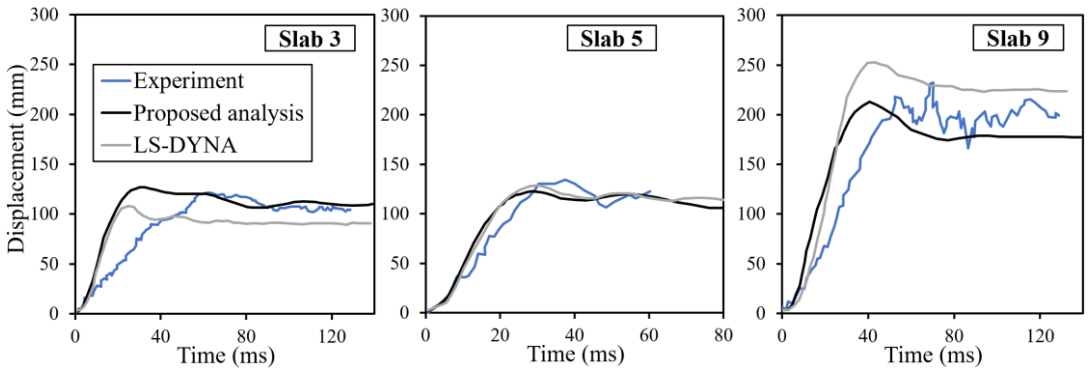

Fig. 9 Displacement-time responses of slabs tested by Robert and Johnson (2009) (1 mm=0.0394 in.)

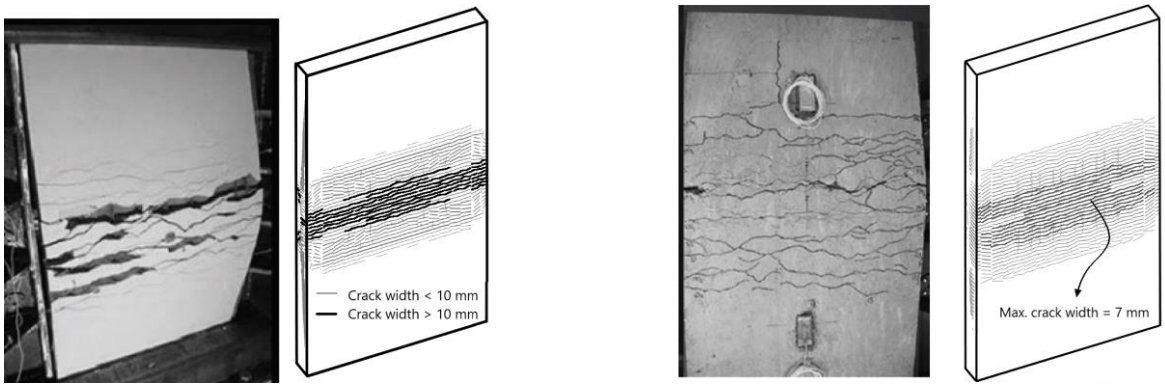

(a) Slab 9 (b) Slab 2

Fig. 10 Comparison of crack patterns obtained from tests and FE analysis for US Army specimens

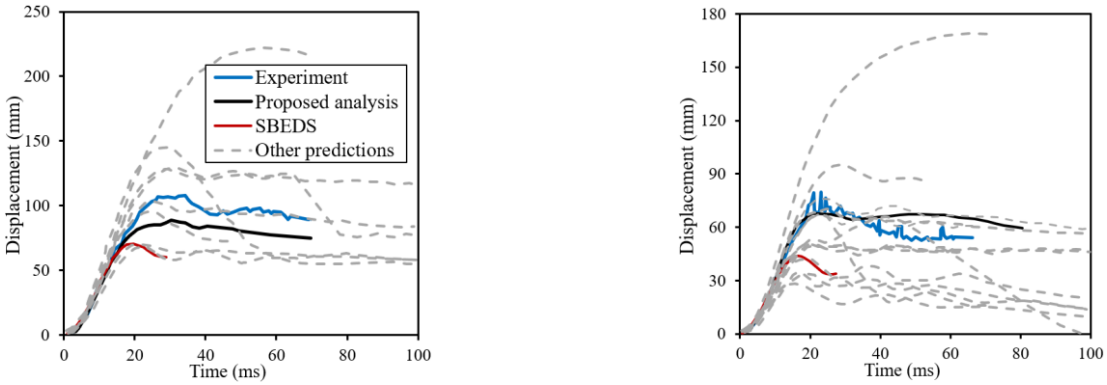

(a) Slab 2 (b) Slab 6

Fig. 11 Displacement-time responses of US Army singly reinforced specimens (1 mm=0.0394 in.)

were generally stiffer than the experimental response for the three slabs. The idealization of the supports may be the possible cause of this discrepancy. For Slab 3, the proposed analysis procedure slightly overestimated the peak displacement, but it computed the residual displacements accurately. On the other hand, the LS-DYNA analysis with the Winfrith concrete model underestimated both the peak and the residual displacements. For Slabs 5 and 9, both analytical methods computed the peak and residual displacements reasonably well. In terms of crack patterns, the proposed FE analysis computed large cross-panel cracks concentrated at the midspan with a maximum width larger than 10 mm (0.39 in.). The crack patterns indicated flexural behavior for all of the specimens which was consistent with the experimentally observed behavior. The crack patterns of Slab 9 obtained from the proposed analysis and the experiment are shown in Fig. 10. It can be seen that the crack distributions are similar to each other.

3.4 US Army singly reinforced specimens

In 2012, two sets of slab specimens were tested at the U.S. Army Engineer Research and Development Center as part of a blast simulation contest sponsored by the American Concrete Institute and the University of Missouri-Kansas City (Thiagarajan 2014). The first set of specimens was made using conventional Grade 60 reinforcement, while the second set had HSLA-V

reinforcement. In this study, the first set of specimens (Slabs 2 and 6) were considered for the validation of the proposed analysis procedure. Details of the specimens are shown in Fig. 8.

The FE modeling procedure was similar to that described for the US Army Singly Reinforced Specimens. The midspan displacement-time histories obtained from the proposed analysis and the experiment for Slabs 2 and 6 are compared in Fig. 11. Additionally, the results are compared against the midspan displacement-time histories submitted by various teams participated in the competition and those obtained from the SDOF Blast Effects Design Spreadsheet (SBEDS) developed by the U.S. Army Corps of Engineers Protective Design Center (USACE-PDC 2019). In Fig. 11, the predictions submitted to the competition are shown with gray dashed curves. It can be seen that most of the teams underestimated the experimental responses of both specimens. For Slab 2, the results submitted by the teams had errors ranging from -37% to 103% in terms of the peak displacement. For Slab 6, the errors varied between -73% and 110%. The simplified SBEDS design approach underestimated the peak displacement for both specimens. While the proposed analysis underestimated the response of Slab 2, for Slab 6 it accurately computed the structural response. The underestimation of displacements for Slab 2 can be due to the relatively higher damping ratio assigned to this model to achieve numerical stability.

The crack patterns obtained from the proposed analysis and the experiment at the peak displacement for Slab 2 are shown in Fig. 10. It can be seen that the crack patterns are in good agreement with each other. The maximum crack width computed by the analysis for Slab 2 and Slab 6 was 7 mm and 6 mm, respectively, located at the midspan of the specimens.

4. Conclusions

A macro-modeling dynamic analysis procedure was developed based on a smeared rotating crack model for modeling of reinforced and prestressed concrete panels under blast loads and implemented within the framework of a 3D nonlinear FE analysis program. The proposed analysis procedure was verified by modeling 14 blast tests from various sources reported in the literature. All the analyses were conducted using simple finite element meshing techniques with reasonable mesh sizes and predefined material models requiring only basic input parameters. No fine-tuning of the analysis parameters or material modeling was undertaken. The work presented in this study supports the following conclusions:

1. The macro-modeling approach developed on the basis of the DSFM model can be used as a viable analysis procedure for the performance assessment of reinforced and prestressed concrete structures under blast loads. Compared to the alternative finely detailed hydrocodes, the proposed approach reduces the calibration and assumptions involved in the modeling process and material characterization and requires less modeling efforts.
2. Newmark's time integration method can successfully be employed within the context of the total-load secant stiffness-based solution algorithm for high-frequency dynamic analysis under blast loading. With the formulation presented, other similar static analysis procedures can also be enhanced with the blast analysis capability.
3. Overall, the results of the proposed macro-modeling analysis procedure were in good agreement with the experimental observations in terms of failure mode, peak displacement, damage condition, and crack locations. The ratio of the predicted-to-measured peak displacement for the 14 tests examined had a mean of 0.94 and a coefficient of variation of 13.8%. For the Jacques (2011), Robert and Johnson (2009), and Thiagarajan (2014) specimens which were tested under a well-defined simply supported boundary condition, the predictions were more accurate (mean=0.95 and COV=9.6%). Capturing the response of the Dunkman *et al.* (2009) specimens was more challenging because of the uncertainty in the degree of rotational fixity of the end support condition used in the test. Assuming that the specimens were fully restrained against rotation at low magnitude blasts, while the end supports were not effective in preventing the rotation of the specimen at high magnitude blasts resulted in reasonably accurate peak displacement predictions (mean=0.98 and COV=16.3%). The analysis results show that special care must be given in modeling the end support condition to accurately predict the response of the specimens. In terms of the crack pattern, the proposed analysis procedure captured the width and distribution of cracks which were mostly concentrated at the midspan and were perpendicular to the bending plane reasonably well. It also predicted flexural failure for all the specimens which was consistent with the failure mode observed in the tests.
4. The proposed analysis yielded more accurate results than those obtained from simplified SDOF methods. It also provided more information about the structural response (crack patterns, failure mode, rebound displacement) than the simplified methods available in the literature. Additionally, the proposed analysis was able to provide the same level of accuracy as that obtained from complex LS-DYNA hydrocode models with substantially fewer elements (by an order of magnitude or more) and only requiring basic concrete material properties.
5. With the proposed analysis procedure, using element erosion is not recommended for modeling panels where flexural behavior is the governing mechanism and experience a uniform damage. Crack width and angle calculations inherently included in the DSFM are sufficient for capturing the damage condition of the target. For tests where the local damage is significant, element erosion may be necessary.

References

Akkaya, Y., Guner, S. and Vecchio, F.J. (2019), "Constitutive model for inelastic buckling behavior of reinforcing bars", *ACI Struct. J.*, **116**(2), 195-204. https://doi.org/10.14359/51711143.

Bentz, E.C. (2005), "Explaining the riddle of tension stiffening models for shear panel experiments", *ASCE J. Struct. Eng.*, **131**(9), 1422-1425. https://doi.org/10.1061/(ASCE)0733-9445(2005)131:9(1422).

Bhuyan, K. and Sharma, H. (2024), "Probabilistic capacity models and fragility estimate for NRC and UHSC panels subjected to contact blast", *Reliab. Eng. Syst. Saf.*, **242**, 109683. https://doi.org/10.1016/j.ress.2023.109683.

Brannon, R.M. and Leelavanichkul, S. (2009), "Survey of four damage models for concrete", Report No. SAND2009-5544; Sandia National Laboratories, Albuquerque, NM, USA.

Comite Euro International du Beton (1993), *CEB-FIP Model Code 1990*, Thomas Telford Ltd, London, UK.

Cook, R.D., Malkus, D.S. and Plesha, M.E. (1989), *Concepts and Applications of Finite Element Analysis*, 3rd Edition, Wiley, New York, NY, USA.

Cotsovos, D.M. and Pavlovic, M.N. (2008), "Numerical investigation of concrete subjected to high rates of uniaxial tensile loading", *Int. J. Impact Eng.*, **35**, 319-335. https://doi.org/10.1016/j.ijimpeng.2007.03.006.

Dauj, S. (2020), "Prediction of concrete spall damage under blast: Neural approach with synthetic data", *Comput. Concrete*, **26**(6), 533-546. https://doi.org/10.12989/cac.2020.26.6.533.

Dunkman, D.A., Yousef, A.E.A., Karve, P.M. and Williamson, E.B. (2009), "Blast performance of prestressed concrete panels", *Structures Congress 2009: Don't Mess with Structural Engineers: Expanding Our Role*, Austin, TX, USA, April-May.

ElMohandes, F. and Vecchio, F.J. (2016), "Reliability of temperature-dependent models for analysis of reinforced concrete members subjected to fire", *ACI Struct. J.*, **113**(3), 481-490. https://doi.org/10.14359/51688605.

Jain, P. and Chakraborty, T. (2018), "Numerical analysis of tunnel in rock with basalt fiber reinforced concrete lining subjected to internal blast load", *Comput. Concrete*, **21**(4), 399-406. https://doi.org/10.12989/cac.2018.21.4.399.

Gang, H. and Kwak, H.G. (2017), "A tensile criterion to minimize FE mesh-dependency in concrete beams under blast loading", *Comput. Concrete*, **20**(1), 1-10. https://doi.org/10.12989/cac.2017.20.1.001.

Gangolua, J., Kumarb, A., Bhuyanb, K. and Sharma, H. (2022), "Performance-based probabilistic capacity models for reinforced concrete and prestressed concrete protective structures subjected to missile impact", *Int. J. Impact Eng.*, **164**, 104207. https://doi.org/10.1016/j.ijimpeng.2022.104207.

Gangolu, J., Daudeville, L., Gangolu, A.R. and Sharma, H. (2023), "Improvement of probabilistic models for prediction of missile-impact effects on reinforced concrete protective panels using an experimental and numerical database", *ASCE J. Perform. Constr. Facil.*, **37**(5), 04023036. https://doi.org/10.1061/JPCFEV.CFENG-4316.

Hoshikuma, J., Kawashima, K., Nagaya, K. and Taylor, A.W. (1997), "Stress-strain model for confined reinforced concrete in bridge piers", *ASCE J. Struct. Eng.*, **123**(5), 624-633. https://doi.org/10.1061/(ASCE)0733-9445(1997)123:5(624).

Iannitti, G., Bonora, N., Curiale, G., De Muro, S., Marfia, S., Ruggiero, A., Sacco, E., Scafati, S. and Testa, G. (2018), "Analysis of reinforced concrete slabs under blast loading", *Struct. Integr. Proc.*, **9**, 272-278. https://doi.org/10.1016/j.prostr.2018.06.035.

Isojeh, B., El-Zeghayar, M. and Vecchio, F.J. (2019), "Numerical analysis of reinforced concrete and steel-fiber concrete elements under fatigue loading", *ASCE J. Struct. Eng.*, **145**(11), 04019126. https://doi.org/10.1061/(ASCE)ST.1943-541X.0002349.

Jacques, E. (2011), "Blast retrofit of reinforced concrete walls and slabs", Master's Thesis, University of Ottawa, Ottawa, Ontario, Canada.

Kong, X.Q., Zhao, Q., Qu, Y.D. and Zhang, W.J. (2018), "Blast response of cracked RC slabs repaired with CFRP composite patch", *KSCE J. Civil Eng.*, **22**(4), 1214-1224. https://doi.org/10.1007/s12205-017-1054-3.

Li, Q.M. and Meng, H. (2003), "About the dynamic strength enhancement of concrete-like materials in a split Hopkinson pressure bar test", *Int. J. Solid. Struct.*, **40**, 343-360. https://doi.org/10.1016/S0020-7683(02)00526-7.

Lin, Y., Shunfeng, G. and Weiliang, J. (2008), "Spallation mechanism of RC slabs under contact detonation", *J. Trans. Tianjin Univ.*, **14**, 464-469. https://doi.org/10.1007/s12209-008-0079-6.

Lin, X., Zhang, Y.X. and Hazell, P.J. (2014), "Modelling the response of reinforced concrete panels under blast loading", *Mater. Des.*, **56**, 620-628. https://doi.org/10.1016/j.matdes.2013.11.069.

Lulec, A. (2017), "Simplified analytical tools for impact and impulsive loading analysis of reinforced concrete structures", Ph.D. Dissertation, University of Toronto, Toronto, Canada.

Malvar, L.J. and Crawford, J.E. (1998), "Dynamic increase factor for steel reinforcing bars", *28th DDESB Seminar*, Orlando, FL, USA, September.

Nam, J.W., Yoon, I.S. and Yi, S.T. (2016), "Numerical evaluation of FRP composite retrofitted reinforced concrete wall subjected to blast load", *Comput. Concrete*, **17**(2), 215-225. https://doi.org/10.12989/cac.2016.17.2.215.

Newmark, N.M. (1959), "A method of computation for structural dynamics", *ASCE J. Eng. Mech. Div.*, **85**(3), 67-94. https://doi.org/10.1061/JMCEA3.0000098.

Palermo, D. and Vecchio, F.J. (2003), "Compression field modelling of reinforced concrete subjected to reversed loading: formulation", *ACI Struct. J.*, **100**(5), 616-625.

Park, G.K., Kwak, H.G. and Filippou, C. (2021), "Hysteretic moment-curvature relations for the analysis of RC flexural members subjected to blast loading", *Comput. Concrete*, **27**(6), 537-548. https://doi.org/10.12989/cac.2021.27.6.537.

Rashad, M. and Yang, T.Y. (2019), "Improved nonlinear modelling approach of simply supported PC slab under free blast load using RHT model", *Comput. Concrete*, **23**(2), 121-131. https://doi.org/10.12989/cac.2019.23.2.121.

Robert, S. and Johnson, C. (2009), "Blast response of conventional and high performance reinforced concrete panels", *Structures Congress 2009: Don't Mess with Structural Engineers: Expanding Our Role*, Austin, TX, USA, April-May.

Saatci, S. and Vecchio, F.J. (2009), "Nonlinear finite element modeling of reinforced concrete structures under impact loads", *ACI Struct. J.*, **106**(5), 717-725. https://doi.org/10.14359/51663112.

Seckin, M. (1981), "Hysteretic behaviour of cast-in-place exterior beam-column-slab subassemblies", Ph.D. Dissertation, University of Toronto, Toronto, Ontario, Canada.

Tai, Y.S., Chu, T.L., Hu, H.T. and Wu J.Y. (2011), "Dynamic response of a RC slab subjected to air blast load", *Theoret. Appl. Fract. Mech.*, **56**(3), 140-147. https://doi.org/10.1016/j.tafmec.2011.11.002.

Thiagarajan, G. and Johnson, C.F. (2014), "Experimental behavior of reinforced concrete slabs subjected to shock loading", *ACI Struct. J.*, **111**(6), 1407-1417. https://doi.org/10.14359/51686970.

Thiagarajan, G., Kadambi, A.V., Robert, S. and Johnson, C.F. (2015), "Experimental and finite element analysis of doubly reinforced concrete slabs subjected to blast loads", *Int. J. Impact Eng.*, **75**, 162-173. https://doi.org/10.1016/j.ijimpeng.2014.07.018.

USACE-PDC (2019), "Single-degree-of-freedom blast effects design spreadsheet (SBEDS)", Report No. 4213; U.S. Army Corps of Engineers, Protective Design Center, Washington,

D.C., USA.
Vecchio, F.J. (2000), "Disturbed stress field model for reinforced concrete: Formulation", *ASCE J. Struct. Eng.*, **126**(9), 12-20. https://doi.org/10.1061/(ASCE)0733-9445(2000)126:9(1070).
Vecchio, F.J. and Collins, M.P. (1993), "Compression response of cracked reinforced concrete", *ASCE J. Struct. Eng.*, **119**(12), 3590-3610. https://doi.org/10.1061/(ASCE)0733-9445(1993)119:12(3590).
Vecchio, F.J. and Selby, R.G. (1991), "Towards compression field analysis of reinforced concrete solids", *ASCE J. Struct. Eng.*, **117**(6), 1740-1758. https://doi.org/10.1061/(ASCE)0733-9445(1991)117:6(1740).
Xu, K. and Lu, Y. (2006), "Numerical simulation study of spallation in reinforced concrete plates subjected to blast loading", *Comput. Struct.*, **84**(5), 431-438. https://doi.org/10.1016/j.compstruc.2005.09.029.
Yan, J., Liu, Y., Xu, Z., Li, Z. and Huang, F. (2020), "Experimental and numerical analysis of CFRP strengthened RC columns subjected to close-in blast loading", *Int. J. Impact Eng.*, **146**, 103720. https://doi.org/10.1016/j.ijimpeng.2020.103720.
Zhao, C.F. and Chen, J.Y. (2013), "Damage mechanism and mode of square reinforced concrete slab subjected to blast loading", *Theoret. Appl. Fract. Mech.*, **63**, 54-62. https://doi.org/10.1016/j.tafmec.2013.03.006.

CC